Direct reconstruction of cardiac PET kinetic parametric images using a preconditioned conjugate gradient approach

Yothin Rakvongthai, Jinsong Ouyang, Bastien Guerin,[a] Quanzheng Li, Nathaniel M. Alpert, and Georges El Fakhri[b]
Center for Advanced Medical Imaging Sciences, Division of Nuclear Medicine and Molecular Imaging, Massachusetts General Hospital, Boston, Massachusetts 02114 and Department of Radiology, Harvard Medical School, Boston, Massachusetts 02114

(Received 31 December 2012; revised 2 August 2013; accepted for publication 10 August 2013; published 5 September 2013)

Purpose: Our research goal is to develop an algorithm to reconstruct cardiac positron emission tomography (PET) kinetic parametric images directly from sinograms and compare its performance with the conventional indirect approach.
Methods: Time activity curves of a NCAT phantom were computed according to a one-tissue compartmental kinetic model with realistic kinetic parameters. The sinograms at each time frame were simulated using the activity distribution for the time frame. The authors reconstructed the parametric images directly from the sinograms by optimizing a cost function, which included the Poisson log-likelihood and a spatial regularization terms, using the preconditioned conjugate gradient (PCG) algorithm with the proposed preconditioner. The proposed preconditioner is a diagonal matrix whose diagonal entries are the ratio of the parameter and the sensitivity of the radioactivity associated with parameter. The authors compared the reconstructed parametric images using the direct approach with those reconstructed using the conventional indirect approach.
Results: At the same bias, the direct approach yielded significant relative reduction in standard deviation by 12%–29% and 32%–70% for 50×10^6 and 10×10^6 detected coincidences counts, respectively. Also, the PCG method effectively reached a constant value after only 10 iterations (with numerical convergence achieved after 40–50 iterations), while more than 500 iterations were needed for CG.
Conclusions: The authors have developed a novel approach based on the PCG algorithm to directly reconstruct cardiac PET parametric images from sinograms, and yield better estimation of kinetic parameters than the conventional indirect approach, i.e., curve fitting of reconstructed images. The PCG method increases the convergence rate of reconstruction significantly as compared to the conventional CG method. [http://dx.doi.org/10.1118/1.4819821]

Key words: direct estimation, preconditioned conjugate gradient, kinetic modeling, parametric imaging, dynamic PET

1. INTRODUCTION

Parametric imaging from dynamic positron emission tomography (PET) makes it possible to extract physiological information via kinetic modeling of the time evolution of the activity concentration, i.e., time-activity curve (TAC).[1] In conventional parametric imaging, frame-by-frame images are reconstructed first followed by curve-fitting TACs voxel-wise to estimate kinetic parameters.[2,3] This so-called indirect approach typically results in very noisy parametric images.

Direct reconstruction was first proposed by Snyder[4] and Carson and Lange,[5] and has recently gained attention as an alternative approach for parametric imaging. In the direct approach, kinetic parameters are estimated directly from the measured data. The direct approach has potential to reduce noise in parametric images because it does not require two assumptions which are made in the indirect approach. First, curve-fitting the reconstructed image with the kinetic model assumes that noise in the image domain follows a model (e.g., Gaussian model in the case of least-square curve-fitting). However, this noise model in the image domain is difficult to estimate.[6,7] Second, fitting in the indirect approach is performed voxel-wise; therefore, intervoxel correlation is ignored.[7]

There have been several studies on direct parametric reconstruction in dynamic PET imaging. Most of the existing algorithms for direct reconstruction are for linear models, such as spectral bases,[8–10] B-splines,[11,12] and the Patlak model.[13–15] The linearity of the TAC model allows the algorithms developed for static PET image reconstruction to be extended and used for direct reconstruction of linear parametric images. For example, the maximum-likelihood expectation-maximization (ML-EM) algorithm was used by Matthews *et al.*[8] and Tsoumpas *et al.*[14] A preconditioned conjugate gradient (PCG) algorithm in the maximum *a posteriori* (MAP) framework was presented by Wang *et al.*[13] (and its nested algorithm for the ML reconstruction[16] to improve the convergence rate). Recently, the EM algorithm with bound constraints was proposed to use for direct Patlak parametric estimation by Rahmim *et al.*[17] Most of these algorithms

require linearization of the kinetic model.[13,14] In this work, we focus on direct reconstruction algorithms of nonlinear kinetic models.

One main difficulty of the direct approach with nonlinear kinetic models is the complexity of the optimization algorithm owing to the nonlinearity of the model with respect to the parameters.[2,3] Unlike linear models, the log-likelihood function for the nonlinear models in general is not concave, and does not guarantee global convergence in the ML framework. The ML-EM algorithm was used by Carson and Lange[5] (and later extended by Yan *et al.*[18]) for a one-tissue compartmental model. The parametric iterative coordinate descent (PICD) method was applied by Kamasak *et al.*[19] for direct parametric reconstruction of a two-tissue compartmental model. Moreover, the surrogate function technique was deployed for direct reconstruction by Wang and Qi[7] with the paraboloidal surrogate, and by the same authors with the EM surrogate.[20] Comprehensive reviews on the topic were presented by Tsoumpas *et al.*[3] and Rahmim *et al.*[2]

In this work, we have developed a novel direct PET parametric reconstruction approach based on a PCG algorithm. Specifically, we chose the preconditioner to be a generalized version of the precondition used in the direct parametric reconstruction for linear models, which imitates the preconditioner for PCG-based image reconstruction in static emission tomography. This preconditioner, which was called the EM preconditioner,[21] is a diagonal matrix derived implicitly from the EM algorithm.[22] We applied the proposed algorithm to myocardial blood flow estimation for a PET perfusion study. The optimization algorithm for direct parametric reconstruction in this work was implemented on the region of interest (ROI)-targeted reconstruction where we updated parameters only in voxels in the ROI to have feasible computation time. We studied the performance of the estimation of kinetic parameters and the convergence behavior of the reconstruction using our method.

We would like to point out that the aim of this work is to investigate the improvement of the direct parametric reconstruction as compared to the existing standard indirect approach, which is the standard OSEM method together with kinetic model fitting. Additionally, in order to make a comparison between the direct and the indirect approaches in terms of bias and standard deviation, we need to know the true values of kinetic parameters. Therefore, we decided to perform simulation studies using realistic kinetic parameters in this work.

2. MATERIALS AND METHODS

In dynamic PET imaging, the data which contain N_i sinogram bins and are measured in N_m time frames are modeled as a set of Poisson random variables, i.e.,

$$y_{im} \sim \text{Poisson}\{\bar{y}_{im}\}, \quad i = 1, \ldots, N_i; \quad m = 1, \ldots, N_m, \tag{1}$$

where y_{im} is the mean of the number of detected events in sinogram bin i at time frame m, $\bar{y}_{im}$, is related to the activity concentration distribution $\{x_{jm}\}$ at time frame m via the system matrix

$$\bar{y}_{im} = \sum_{j=1}^{N_j} A_{ij} x_{jm}, \tag{2}$$

where A_{ij}, which is the probability of a positron emitted from voxel j to be detected sinogram in bin i, is the (i, j)th element of the system matrix $\mathbf{A} \in R^{N_i \times N_j}$, and N_j is the number of voxels. The activity distribution x_{jm} at voxel j in time frame m can be computed as the accumulated concentration $x_{jm} = \int_{t_{m,s}}^{t_{m,e}} x_j(t) e^{-\lambda t} dt$, where $t_{m,s}$ and $t_{m,e}$ are the start and end times of time frame m, λ is the decay constant of the radiotracer, and $x_j(t)$ is the activity concentration in voxel j at time instant t. This concentration in voxel j can be modeled by $x_j(t) = f(t; \mathbf{k}_j)$, where $\mathbf{k}_j = [k_{j1}, k_{j2}, \ldots, k_{jN_l}]^T$ is the vector of kinetic model's parameters, N_l is the number of kinetic parameters for each TAC, and ^{T} denotes the transpose of a vector or a matrix. For example, we have $\mathbf{k}_j = [K_1^{(j)}, k_2^{(j)}]^T$ for a one-tissue compartmental model.

The aim of kinetic analysis is to estimate these kinetic parameters. There are two main analysis approaches: direct and indirect.

2.A. Conventional indirect approach

The indirect approach consists of two steps: image reconstruction frame-by-frame and curve fitting. The image reconstruction at each time frame can be performed by maximizing the log-likelihood term

$$\hat{\mathbf{x}}_m = \arg\max_{\mathbf{x}_m \geq 0} L(\mathbf{y}_m | \mathbf{x}_m), \tag{3}$$

where $\hat{\mathbf{x}}_m$ is the reconstructed image at frame m, and

$$L(\mathbf{y}_m | \mathbf{x}_m) = \sum_{i=1}^{N_i} (y_{im} \log \bar{y}_{im}(\mathbf{x}_m) - \bar{y}_{im}(\mathbf{x}_m)). \tag{4}$$

Kinetic analysis is then performed by curve-fitting the TAC in each voxel using a nonlinear least-square fitting

$$\hat{\mathbf{k}}_j = \arg\min_{\mathbf{k}_j} \sum_{m=1}^{N_m} w_m (\tilde{x}_{jm} - z_{jm}(\mathbf{k}_j))^2, \tag{5}$$

where $\tilde{x}_{jm} = \hat{x}_{jm}/\Delta t_m$, $z_{jm}(\mathbf{k}_j) = \frac{1}{\Delta t_m} \int_{t_{m,s}}^{t_{m,e}} f(t; \mathbf{k}_j) e^{-\lambda t} dt$, in which $\Delta t_m = t_{m,e} - t_{m,s}$, is the average concentration in voxel j at time frame m, w_m is the weighting factor which herein is chosen to be the squared frame duration divided by the total counts in that frame.[23] This nonlinear least square problem can be solved using the Levenberg-Marquardt algorithm.[7]

2.B. Direct approach

The direct approach integrates the kinetic modeling within the image reconstruction. By relating the dynamic sinogram to the parametric image via the dynamic image, the parametric reconstruction can be performed by maximizing the log-likelihood function (ignoring the constant term)

$$\hat{\mathbf{k}} = \arg\max_{\mathbf{k}} L(\mathbf{y}|\mathbf{k}), \tag{6}$$

where $L(\mathbf{y}|\mathbf{k}) = \sum_{m=1}^{N_m}\sum_{i=1}^{N_i}(y_{im}\log\bar{y}_{im}(\mathbf{k}) - \bar{y}_{im}(\mathbf{k}))$, $\bar{y}_{im}(\mathbf{k}) = \sum_{j=1}^{N_j} A_{ij}x_{jm}(\mathbf{k}_j)$ is the mean of the number of detected events in sinogram bin i acquired throughout time frame m, and $x_{jm}(\mathbf{k}_j)$ is the image voxel value due to the kinetic parameters $\mathbf{k}_j$. It should be noted that, in general, the log-likelihood function $L(\mathbf{y}|\mathbf{k})$ is non-concave with respect to the parametric images $\mathbf{k}$. Therefore, any convex optimization algorithm can only guarantee convergence to a local optimum.

2.B.1. Direct parametric reconstruction with the preconditioned conjugate gradient (PCG) algorithm

2.B.1.a. PCG algorithm for linear parametric reconstruction. In the framework for linear models, the TAC at each voxel is

$$x_{jm} = \sum_{l=1}^{N_l} B_{ml}\theta_{jl}, \tag{7}$$

where B_{ml} is the value lth basis function at time frame m, θ_{jl} is kinetic parameter of the lth basis function in voxel j. The kinetic parameters can be estimated using the maximum likelihood criterion:

$$\hat{\boldsymbol{\theta}} = \underset{\boldsymbol{\theta}}{\operatorname{argmax}} \sum_{m=1}^{N_m}\sum_{i=1}^{N_i}(y_{im}\log\bar{y}_{im}(\boldsymbol{\theta}) - \bar{y}_{im}(\boldsymbol{\theta})), \tag{8}$$

where $\bar{y}_{im}(\boldsymbol{\theta}) = \sum_{j=1}^{N_j}\sum_{l=1}^{N_l} A_{ij}B_{ml}\boldsymbol{\theta}_{jl}$. Due to the linearity with respect to the parameters of the TAC model, it can be shown that the EM algorithm for linear parametric image reconstruction is equivalent to the scaled gradient ascent method.[13] The PCG algorithm can be used to accelerate the EM algorithm in linear parametric reconstruction as well. The PCG method can be described in the following iterative steps:[16,24]

Step 1: Compute the current update direction $\mathbf{d}^{[n]} = \mathbf{Q}^{[n]}\mathbf{g}^{[n]}$, where $\mathbf{g}^{[n]} = \{g_{jl}^{[n]}\}$ is the gradient vector, and the preconditioner, $\mathbf{Q}^{[n]} = \operatorname{diag}\{q_{jl}^{[n]}\}$, is a diagonal matrix with

$$q_{jl}^{[n]} = \frac{\theta_{jl}^{[n]}}{s_j\left(\sum_{m=1}^{N_m} B_{ml}\right)}, \tag{9}$$

where $s_j = \sum_{i=1}^{N_i} A_{ij}$ is the sensitivity of voxel j. Note that this $\mathbf{Q}^{[n]}$ is the parametric version of the EM preconditioner.

Step 2: Compute the conjugate direction $\mathbf{a}^{[n]} = \mathbf{d}^{[n]} + \gamma^{[n-1]}\mathbf{a}^{[n-1]}$, where $\mathbf{a}^{[0]} = \mathbf{d}^{[0]}$ initially, and $\gamma^{[n-1]}$ is chosen according to the Polak-Ribiere form:[16,24]

$$\gamma^{[n-1]} = \frac{(\mathbf{g}^{[n]} - \mathbf{g}^{[n-1]})^T\mathbf{d}^{[n]}}{(\mathbf{g}^{[n-1]})^T\mathbf{d}^{[n-1]}}. \tag{10}$$

Step 3: Calculate the new estimate $\boldsymbol{\theta}^{[n+1]} = \boldsymbol{\theta}^{[n]} + \alpha^{[n]}\mathbf{a}^{[n]}$, where $\alpha^{[n]}$ is calculated from a line search

$$\alpha^{[n]} = \underset{\alpha}{\operatorname{argmax}}\ L(\mathbf{y}|\boldsymbol{\theta}^{[n]} + \alpha\mathbf{a}^{[n]}). \tag{11}$$

2.B.1.b. The new preconditioner for nonlinear parametric reconstruction. To find the preconditioner for PCG-based nonlinear parametric reconstruction, we first modify the denominator in Eq. (9) in a more general form as

$$q_{jl}^{[n]} = \frac{\theta_{jl}^{[n]}}{\left(\sum_{m=1}^{N_m}\frac{\partial x_{jm}}{\partial\theta_{jl}}\right)\left(\sum_{i=1}^{N_i} A_{ij}\right)} = \frac{\theta_{jl}^{[n]}}{\left(\sum_{m=1}^{N_m}\sum_{i=1}^{N_i}\frac{\partial\bar{y}_{jm}}{\partial\theta_{jl}}\right)}, \tag{12}$$

i.e., the denominator is the sensitivity of the mean detected counts with respect to the parameter as suggested by Li *et al.*[12] Inspired by this definition, we proposed the preconditioner for the nonlinear case to be the diagonal matrix whose diagonal entries are ratio of the parameter and the sensitivity of mean detected counts due to that parameter, i.e.,

$$q_{jl}^{[n]} = \frac{k_{jl}^{[n]}}{\left|\sum_{m=1}^{N_m}\sum_{i=1}^{N_i}\frac{\partial\bar{y}_{jm}}{\partial k_{jl}}\right|_{\mathbf{k}_j=\mathbf{k}_j^{[n]}}} = \frac{k_{jl}^{[n]}}{s_j\left|\sum_{m=1}^{N_m}\frac{\partial x_{jm}}{\partial k_{jl}}\right|_{\mathbf{k}_j=\mathbf{k}_j^{[n]}}}. \tag{13}$$

We used the absolute value in the denominator so that the preconditioner is a symmetric positive definite matrix to guarantee convergence.[25] In the case of one-tissue compartmental models, the TAC in voxel j follows the model $x_j(t;\ \mathbf{k}_j) = K_1^{(j)}[C_p(t) * e^{-k_2^{(j)}t}]$, where $C_p(t)$ denotes the plasma input function, i.e., in this case $\mathbf{k}_j = [k_{j1},\ k_{j2}]^T = [K_1^{(j)},\ k_2^{(j)}]^T$. Therefore, the diagonal elements of the proposed preconditioner in Eq. (13) for one-tissue compartmental models are given by

$$q_{j1}^{[n]} = \frac{k_{j1}^{[n]}}{s_j\left(\sum_{m=1}^{N_m}\int_{t_{m,s}}^{t_{m,e}}[C_p(\tau) * e^{-k_{j2}\tau}]\,e^{-\lambda\tau}d\tau\right)_{\mathbf{k}_j=\mathbf{k}_j^{[n]}}},$$

$$q_{j2}^{[n]} = \frac{k_{j2}^{[n]}}{s_j\left(\sum_{m=1}^{N_m}\int_{t_{m,s}}^{t_{m,e}}k_{j1}[\tau C_p(\tau) * e^{-k_{j2}\tau}]\,e^{-\lambda\tau}d\tau\right)_{\mathbf{k}_j=\mathbf{k}_j^{[n]}}}. \tag{14}$$

Note that the calculation of Eq. (13) does not require significant additional computation time since the partial derivatives in the denominator have already been computed in the gradient calculation step.

Besides using the proposed matrix as the preconditioner, the PCG algorithm for nonlinear case proceeds as previously described for linear case in Sec. 2.B.1.a.

2.B.2. Algorithm implementation

Because the maximization of Eq. (6) with respect to the parametric images $\mathbf{k}$ is an ill-posed problem, a regularization term is added in the total cost function to stabilize the optimization. The kinetic parameters are estimated using

$$\hat{\mathbf{k}} = \underset{\mathbf{k}}{\operatorname{argmax}}\ \Phi(\mathbf{k}), \quad \Phi(\mathbf{k}) = L(\mathbf{y}|\mathbf{k}) - \beta U(\mathbf{k}). \tag{15}$$

The regularization term $U(\mathbf{k})$, which penalizes the roughness, can act either on the parametric images $\mathbf{k}$ or on the images $\mathbf{x}_m(\mathbf{k})$, and β is a regularization parameter, which controls the

penalty. In this report, we used the image domain penalty because this introduces only one regularization parameter instead of N_l. We chose the regularization term to be the scaled sum of the squared differences among neighborhoods in the image domain, i.e., the regularization term is of the form

$$U(\mathbf{k}) = U(\mathbf{x}(\mathbf{k})) = \sum_{m=1}^{N_m}\sum_{j=1}^{N_j}\sum_{p\in N(j)}\frac{1}{2(\Delta t_m)^2}(x_{jm}(\mathbf{k}) - x_{pm}(\mathbf{k}))^2, \quad (16)$$

where $N(j)$ is the neighborhood of voxel j.

We selected the ROI, in which a kinetic model f can be applied, and maximized Eq. (15) only in the ROI, i.e., we updated only voxels in the ROI. In this way, the computation time for the optimization algorithm is significantly reduced as compared to the non-ROI optimization because of relatively smaller number of optimization parameters. This ROI optimization approach corresponds to replacing the projection operation, $\bar{y}_{im}(\mathbf{k}) = \sum_{j=1}^{N_j} A_{ij}x_{jm}(\mathbf{k}_j)$, in $L(\mathbf{y}|\mathbf{k})$ of Eq. (6) by $\sum_{j\in\text{ROI}} A_{ij}x_{jm}(\mathbf{k}_j) + \sum_{j\notin\text{ROI}} A_{ij}\hat{x}_{jm}$, where $\hat{x}_{jm}$ is the reconstructed image at time frame m as defined in Sec. 2.B. Note that another type of ROI-based reconstruction for static tomographic reconstruction has been previously discussed (see also Clackdoyle and Defrise[26]).

Our PCG algorithm must apply a non-negativity constraint on all the kinetic parameters. Specifically, in each iteration, if $\mathbf{k}_j^{[n]} < \varepsilon$ (small positive value) and $\mathbf{a}_j^{[n]} < 0$, then $\mathbf{a}_j^{[n]} = 0$ is used to prevent elements of $\mathbf{k}_j^{[n]}$ from being negative. We then applied Armijo's rule[27] to perform an inexact line search to obtain an acceptable step size of the optimization problem:

$$\alpha^{[n]} = \underset{l^{[n]}\le\alpha\le u^{[n]}}{\text{argmax}}\ L(\mathbf{y}|\mathbf{k}^{[n]} + \alpha\mathbf{a}^{[n]}), \quad (17)$$

where $l^{[n]}$ and $u^{[n]}$ are the lower and upper bounds, respectively, on α such that $\mathbf{k}^{[n]} + \alpha\mathbf{a}^{[n]}$ is non-negative. We also incorporated the upper bound constraint by performing the second line-search. After the first line search in Eq. (17), we obtained $\tilde{\mathbf{k}}^{[n]}$, which is the truncated version of $\mathbf{k}^{[n]}$ according to $\mathbf{k}^{\max}$ (the vector of the upper bounds). Then the second inexact line search was performed with respect to the optimization problem:

$$\alpha^* = \underset{0\le\alpha\le 1}{\text{argmax}}\ L(\mathbf{y}|\tilde{\mathbf{k}}^{[n]} + \alpha(\mathbf{k}^{[n]} - \tilde{\mathbf{k}}^{[n]})). \quad (18)$$

2.C. Simulated data

We performed simulation studies using a NCAT torso phantom,[28] which includes heart, lungs, liver, and soft-tissue compartments. Thirty-two PET noise realizations were generated. Attenuation and normalization were used in the simulations. We did not account for random and scatter events in this work. The LV myocardium was segmented into 17 standard segments.[29] The time activity curves of all compartments were simulated according to a one-tissue compartmental model with realistic kinetic parameters from previously reported human PET perfusion studies. The simulation data are equivalent to a 13-min dynamic PET scan with the framing scheme of 6 × 5s, 3 × 30s, 5 × 60s, and 3 × 120s frames. The radionuclide decay was not simulated as, in this work, we intended for F-18 tracers (such as F-18 flurpiridaz), which have relatively long half-lives for 13-min long dynamic PET study.

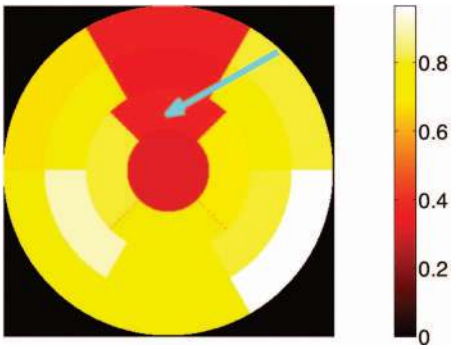

FIG. 1. Reference K_1 polar map in the LV myocardium for our simulation study. Blue arrow indicates defect regions.

We simulated a defect in the anterior wall by lowering K_1 and k_2 values by 50% and 20%, respectively, of the original values. The reference K_1 polar map in LV myocardium is shown in Fig. 1. The blood input function, $C_p(t)$, and TACs for one normal and one defect segments are shown in Fig. 2.

We performed parameter estimation by optimizing the cost function $\Phi(\mathbf{k})$ in Eq. (15), where the ROI mask in the ROI-targeted reconstruction was a dilated myocardium mask. The stopping criterion for our PCG in the simulations is that relative change of the cost function is less than 10^{-6}. The upper bounds on K_1 and k_2 are $K_1^{\max} = 5.0\,\text{min}^{-1}$ and $k_2^{\max} = 0.3\,\text{min}^{-1}$, respectively. We also used a small positive value ε in Sec. 2.B.2 that prevents negativity to be $0.001K_1^{\max}$ for K_1 and $0.001k_2^{\max}$ for k_2.

To address the local maxima problem, the initial values used by our direct approach were set to the kinetic parameters obtained from the indirect approach, which uses frame-by-frame OSEM reconstruction (with 16 subsets and 8 iterations to cope with underconvergence of the OSEM) and voxel-wise curve-fitting. It is worth noting that, in fact, there are several image reconstruction algorithms that can be used in the

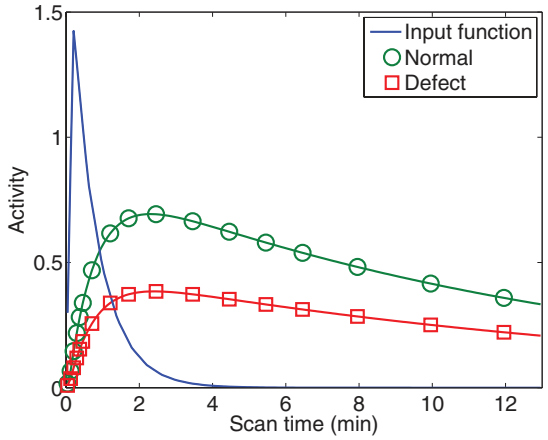

FIG. 2. The blood input function, and TACs of one normal, and one defect segments in the LV myocardium.

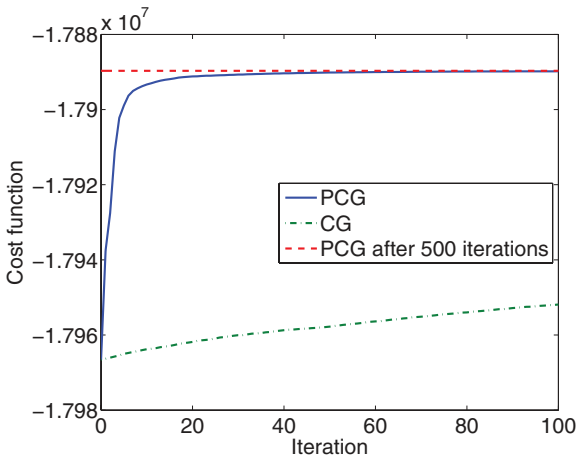

(a) $\beta = 0$

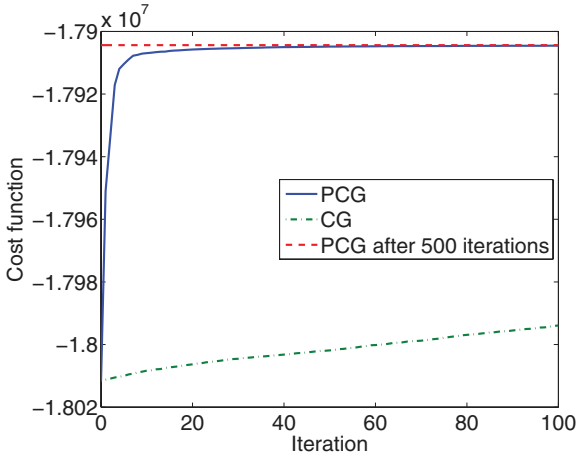

(b) $\beta = 10$

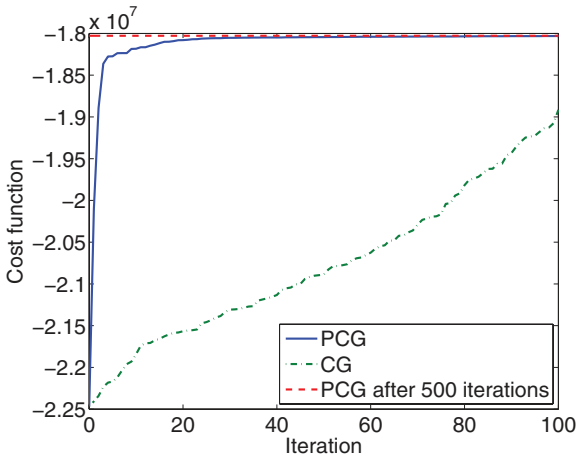

(c) $\beta = 1000$

FIG. 3. (a)–(c) Cost function vs iteration number for the PCG and CG methods.

indirect approach, but we chose to use the OSEM reconstruction since it is close to the image reconstruction algorithm used in current clinical applications.

3. RESULTS

Figure 3 shows the cost function as a function of iteration number for both PCG and CG algorithms for three different β values (0, 10, and 1000) which cover the range of regularization parameters that we used in this work. The cost function after 500 PCG iterations is used as a benchmark for convergence. The proposed PCG algorithm significantly improves convergence rate as compared with the CG algorithm for all β values. After only 10 iterations, the PCG method effectively reached a constant value (with numerical convergence achieved after 40–50 iterations), while more than 500 iterations were needed for CG. The average computation times per iteration for both PCG and CG methods are almost the same (about 9 min on Intel 3.2 GHz Xeon processor).

Next, we looked at the quantification results, where the aim was to estimate the flow (K_1) in the LV myocardium using the direct approach based on PCG algorithm. Figure 4 displays results from the direct approach (at $\beta = 0$ for 50×10^6 counts) by using two different ROI masks in ROI-targeted reconstruction that we mentioned in Sec. 2.B.2. We considered two dilated myocardial masks that represented two levels of dilation [in Fig. 4(a)]; the first mask (Mask 1) had shape very close to the true myocardium while the second one (Mask 2) was a dilated version of the first one. Figures 4(b) and 4(c) show slices of the K_1 mean and standard deviation (SD), respectively, for voxels inside the two masks. The values of voxels outside the mask are displayed as zero. The horizontal and vertical profiles through the defect regions of the mean and SD images are shown in Figs. 4(d) and 4(e). Both masks yielded similar results, especially for voxels in the true myocardium, except for some voxels in which most of them are in Mask 2 but outside Mask 1 (the values for those voxels are displayed as zero). Since the shape of Mask 1 was more complex and closer to the true myocardium's shape, Mask 2 could be obtained easier in practice. In the following, we therefore used Mask 2 as the ROI mask in ROI-targeted reconstruction.

Figures 5(a) and 5(b) show slices of the K_1 mean and SD for both indirect and direct (at $\beta = 0.0$ for 50×10^6 counts) approaches. The horizontal and vertical profiles through the defect regions of the mean and SD images are shown in Figs. 5(c) and 5(d). Both approaches yielded similar bias. However, the direct approach yielded lower noise level than the indirect approach. This was also consistent for the case of 25×10^6 counts as in Figs. 5(e)–5(h).

Figure 6 shows the bias and SD of the estimation of K_1 in one normal segment in the anteroseptal wall, and one defect segment in the anterior wall with different total numbers of counts (50×10^6, 25×10^6, and 10×10^6 counts which correspond to an injection dose of 2.5, 1.25, and 0.5 mCi, respectively). When analyzing the ROI-based results in this work, we assumed that we had the true segmentation where we knew which segment a voxel in the myocardium belongs to. For the direct approach, kinetic parameters were estimated for $\beta = 0$, 10^{-1}, 10^0, 10^1, 10^2. For the indirect approach in this figure, kinetic parameters were obtained by curve-fitting the smoothed reconstructed images, where we used Gaussian filter with parameter σ for $\sigma = 0$, 0.45, 0.9, 1.35, 1.8 mm. To compute the bias and SD values in each ROI, the mean and SD values were those values of estimated K_1 of a voxel from all noise realizations in that ROI (i.e., estimated K_1 values of all voxels in that ROI from all noise realizations were used to compute the

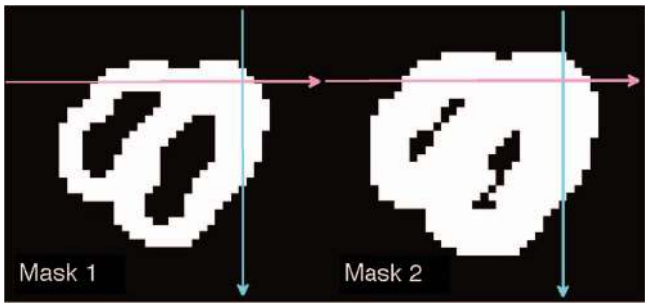

(a) Mask 1 and Mask 2

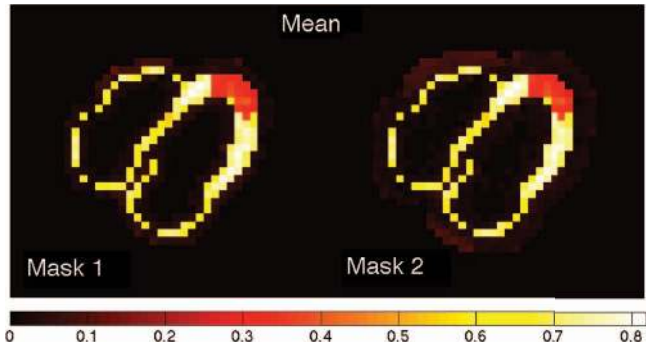

(b) Mean

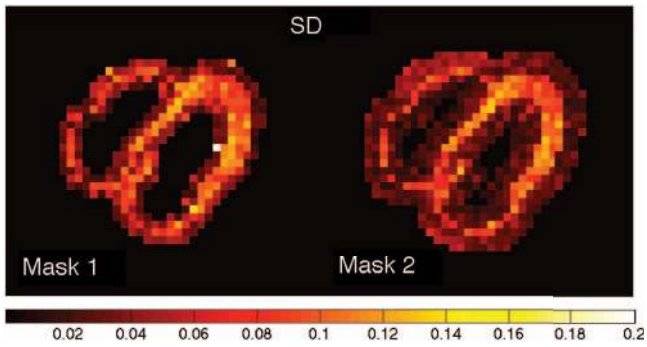

(c) SD

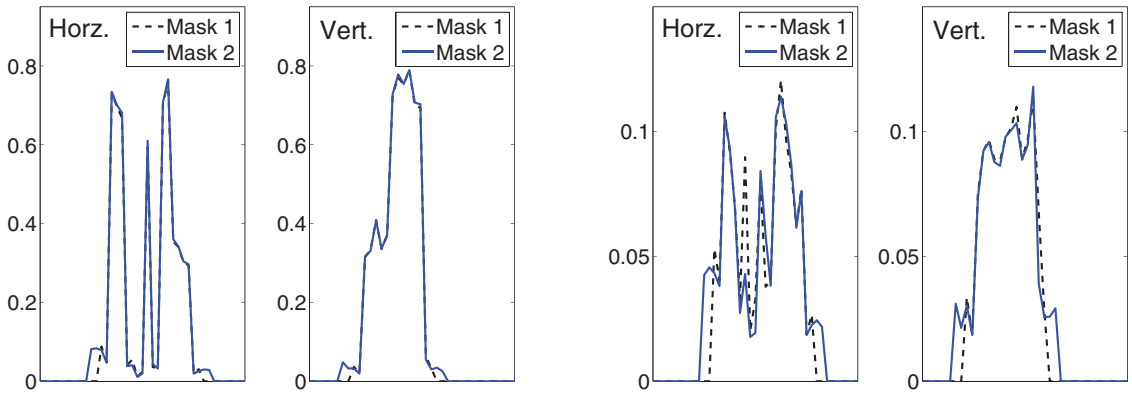

(d) Mean profiles

(e) SD profiles

FIG. 4. (a)–(e) Comparison of the mean and SD images from the direct approach using two different masks for ROI-targeted reconstruction (when $\beta = 0$) in estimating K_1 for 50×10^6 counts. The profiles are horizontal (Horz.) and vertical (Vert.) lines (as in the horizontal and vertical arrows, respectively) through the same myocardial voxels in defect regions for both masks. For each mask, the estimated values from the voxels outside the mask are displayed as zero.

corresponding mean and SD values). We studied the improvement of using the direct approach by calculating SD reduction from what we achieved with the indirect approach with no postfiltering. The bias-SD curve of the direct approach was used to compute the SD for a bias value that equals to the bias of the indirect value. The resulting SD of the direct approach was then used to compute the relative reduction of SD as compared to the indirect approach. At the same bias as the results from the indirect approach with no postreconstruction filtering ($\sigma = 0$ mm), the direct approach reduces SD from 22.7% to 19.2% (3.5 percentage points reduction, or 15.5% relative reduction), 32.8% to 23.3% (9.6% points reduction, or 29.1% relative reduction), 56.2% to 26.1% (30.1% points reduction, or 53.5% relative reduction) in the defect segment for 50×10^6, 25×10^6, and 10×10^6 counts, respectively, compared to the indirect approach. It is also consistent with the normal segments, where the 17-segment polar maps of the SD relative reduction for different total numbers of counts in 17 segments are displayed in Fig. 7. The SD relative reduction is more pronounced for lower counts. Similarly, such reduction is more pronounced in the defect segments compared to the normal ones. The overall relative SD reduction is 17.6%, 23.2%, and 43.1% for 50×10^6, 25×10^6, and 10×10^6 counts, respectively.

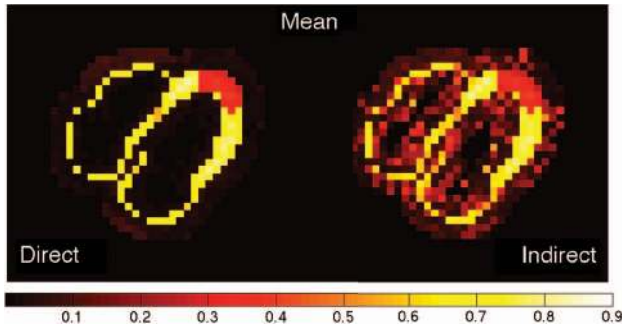

(a) Mean: 50M

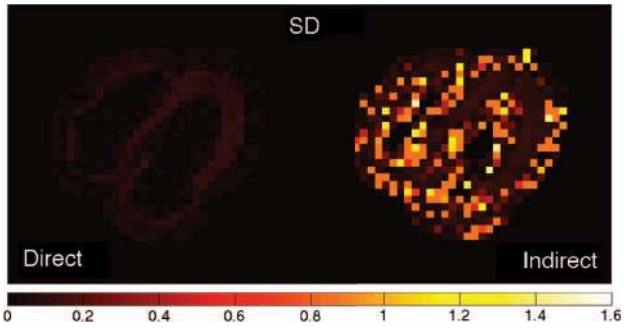

(b) SD: 50M

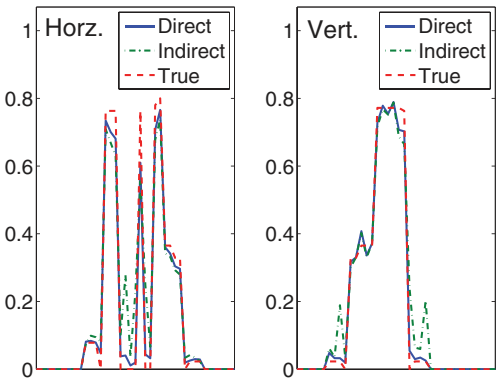

(c) Mean profiles: 50M

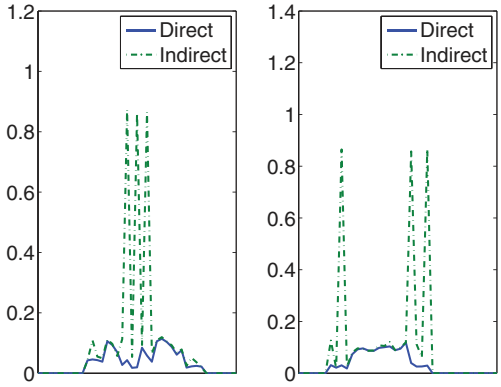

(d) SD profiles: 50M

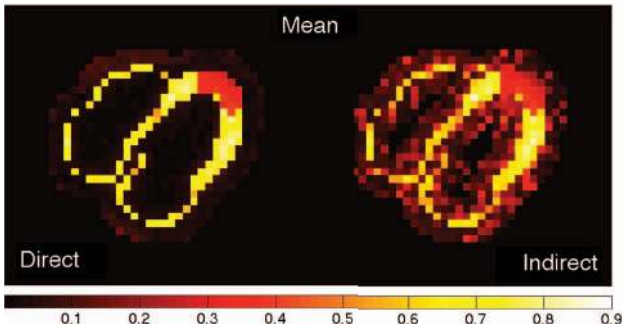

(e) Mean: 25M

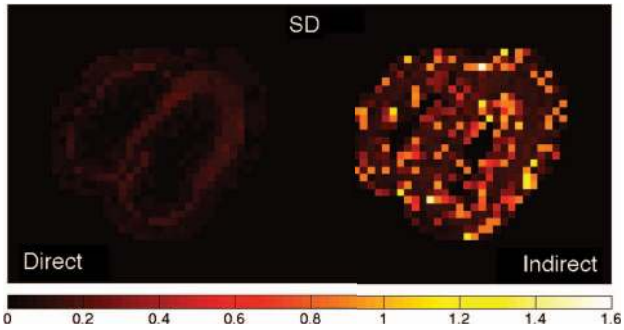

(f) SD: 25M

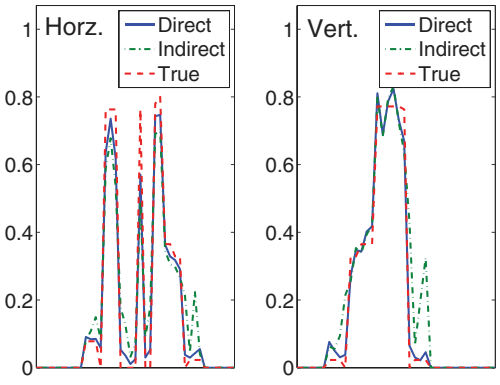

(g) Mean profiles: 25M

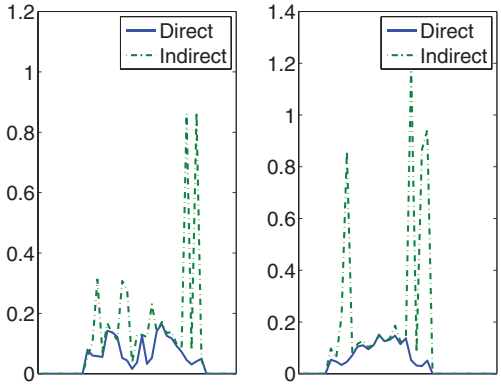

(h) SD profiles: 25M

FIG. 5. (a)–(h) Comparison of the mean and SD images between the direct (when $\beta = 0$) and indirect approaches in estimating K_1 for 50×10^6 and 25×10^6 counts. The profiles are horizontal and vertical lines [as in the horizontal and vertical arrows displayed in Fig. 4(a) for Mask 2] through defect regions. The estimated values from the voxels outside the mask are displayed as zero.

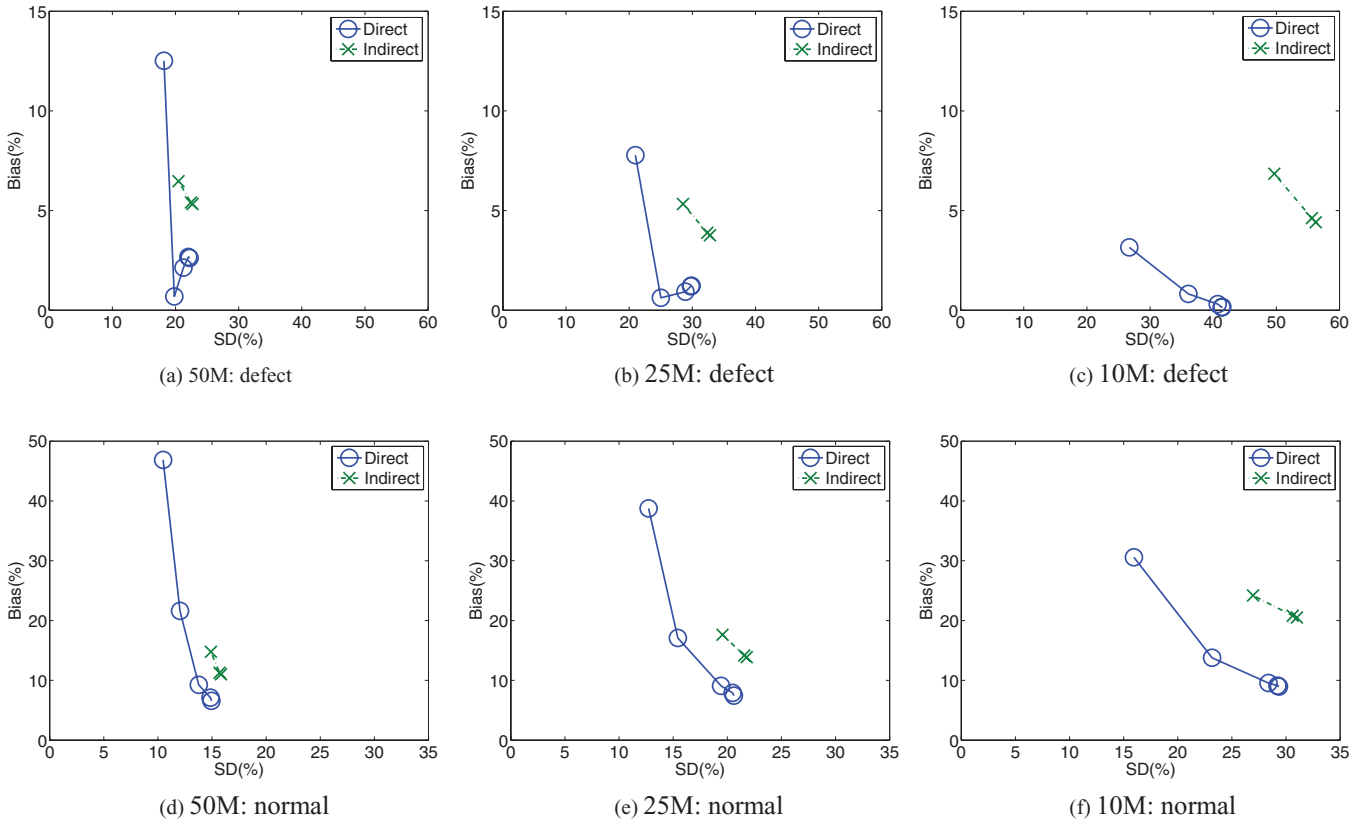

(a) 50M: defect (b) 25M: defect (c) 10M: defect

(d) 50M: normal (e) 25M: normal (f) 10M: normal

FIG. 6. K_1 bias-SD curves for the defect and normal segments in the myocardium for different total number of counts. For the direct approach, the curves were obtained by varying the regularization parameterβ (0 for the right-most point and 100 for the left-most point). The curves of the indirect approach were obtained by varying the parameter σ of the smoothing function (0 mm for the right-most point and 1.8 mm for the left-most point).

Figure. 8 displays the polar plots of the SD relative reduction of the direct approach over the indirect one for two different datasets with the same input function: one without defects (normal kinetic parameters were used) and the other one with defects. The average SD relative reduction in the four defect segments is 23.6% and 14.7% for the dataset with and without defects. The average relative reduction in the other segments is 15.8%, and 17.1% for the dataset with and without defects, respectively. The SD relative reduction is more pronounced in the defect regions compared to normal regions.

4. DISCUSSION

In this work, we proposed a direct nonlinear parametric reconstruction method based on a new PCG approach. The key idea of the proposed method is the preconditioner which is chosen to be a diagonal matrix whose each diagonal entry is the ratio of the parameter and its associated sensitivity of radioactivity. This preconditioner in Eq. (13) reduces to the commonly used preconditioner for PCG-based linear parametric reconstruction, i.e., the proposed preconditioner includes the preconditioner for linear models as a special case.

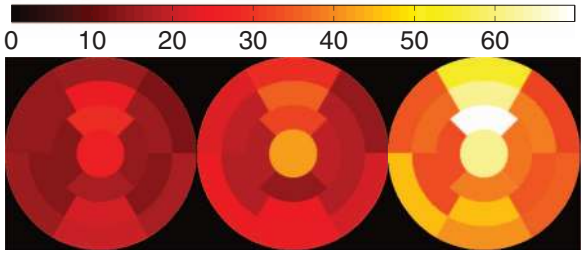

(a) 50M (b) 25M (c) 10M

FIG. 7. SD relative reduction in percentage of K_1 estimation using the direct approach as compared to the indirect approach at different total number of counts. The reduction was compared at the same bias from the indirect approach without postreconstruction filtering.

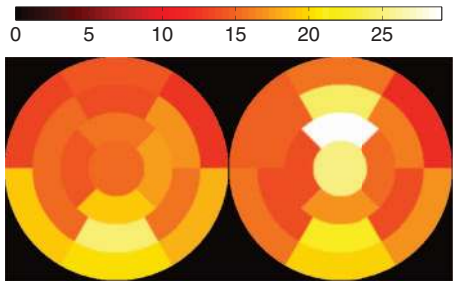

(a) No defect (b) With defects

FIG. 8. SD relative reduction in percentage of K_1 estimation using the direct approach as compared to the indirect approach at 50×10^6 total counts for defect-absent and defect-present studies. The reduction was compared at the same bias from the indirect approach without postreconstruction filtering.

We applied the proposed direct reconstruction method to myocardial blood flow estimation with a one-tissue compartmental modeling. We compared the quantification results to the indirect approach.

In general, fast convergence is desirable for image reconstruction algorithms, especially in direct parametric reconstruction where the algorithms are usually complex due to the nonlinearity relationship between the data and kinetic parameters. The proposed PCG algorithm yields substantially faster convergence (Fig. 3) than the conventional CG algorithm for a wide range of regularization parameters. In terms of computation time, the proposed PCG method requires very little additional computational cost compared to the CG method. The only difference between the PCG and the CG algorithms is Eq. (13), in which the related partial derivatives have already been calculated during the gradient calculation.

In fact, the essence of PCG algorithm is the appropriate preconditioner to improve convergence rate. Ideal case for preconditioner would be the scaled inverse of the Hessian, but is not practical in medical imaging because large imaging dimensions are used.[25] Besides the EM preconditioner frequently used in emission tomography problem, another choice for the preconditioner in general is the inverse of the diagonal of Hessian matrix, which approximates the inverse of Hessian matrix. Even though, in this work the modified parametric version the EM preconditioner is simple and works well in improving convergence rate from the CG, it would be interesting to study convergence comparison with the approximated Hessian inverse or other preconditioners for direct parametric image reconstruction.

In the ROI-targeted reconstruction, the ROI mask had to be chosen to specify the region we would like to perform direct reconstruction. We tested the direct reconstruction with two different masks, both of them were dilated myocardium masks but with different levels of dilation. Both masks yielded very similar estimation results, which imply that our proposed ROI-targeted direct reconstruction is not affected much by the choice of ROI mask at least for two dilated-myocardium-shaped masks. We then chose to use the more dilated mask (Mask 2) since it is easier to obtain due to its less complex shape as compared to Mask 1. In practice, a dilated myocardium mask can be generated by single thresholding of the static PET image. Due to partial volume effect (PVE), we expect such mask should be not too far to the dilated mask that we used in this work.

The simulation studies described in Sec. 3 demonstrated the effectiveness of the proposed direct approach over the conventional indirect approach in estimating the flow in the LV myocardium. Qualitatively, the direct approach yielded less noisy estimation of K_1 than the indirect approach (Fig. 5).

We compared the two approaches by plotting the ROI-based bias-SD curves (Fig. 6). The direct approach allowed the estimation with lower SD without compromising the bias (SD relative reduction of 12%–29% at 50×10^6 counts, the normal count level). This reduction in SD is more visible (Fig. 7) when the total number of counts is lower (SD relative reduction of 32%–70% at 10×10^6 counts), or (Fig. 8) in areas where there are less counts (average SD relative reduction of 15% as compared to 24% in the same segment locations but with lower values of K_1). This pronounced SD relative reduction for low count studies or in defect regions results from the fact that the noise is more properly modeled in the direct approach (see Sec. 1).

The choice of the indirect approach for parametric reconstruction is not unique. Wang and Qi[7] used the same optimization algorithm for both image reconstruction of the indirect approach and the direct parametric reconstruction, except that the former searches in the image space while the latter searches in the parametric space. In this work where the optimization algorithms for the two approaches are different, the indirect approach was chosen to be similar to what is used in clinical applications. Moreover, to cope with the local maxima problem in the direct approach, we initialized the direct reconstruction algorithm by the parametric images from the indirect one. This choice is based on the assumption that the solution obtained from the indirect approach is in the same concave neighborhood as the true parametric images. As a result of this initialization, the OSEM without postfiltering was used in the image reconstruction step of the indirect approach in order to prevent additional bias of the initial values for the direct approach.

It is worth comparing our work to previous studies on direct reconstruction, such as Wang and Qi[7]. In that work, based on the surrogate function techniques, the authors performed direct PET reconstruction with simulation studies for brain imaging applications. In our work, we used the PCG approach in simulation studies for cardiac imaging applications, where the results from the indirect approach (OSEM reconstruction) were used as initial to address the local-maximum problem. Moreover, our direct reconstruction framework is a ROI-targeted reconstruction. In terms of performance reported in Wang and Qi,[7] the mean images of the estimated influx rate (for two-tissue compartmental modeling) for both direct and indirect (which was also based on the surrogate function technique as in the direct case) approaches were very similar, while the SD image of the direct approach had lower values than those from the indirect one. In our work, the mean and SD images from both approaches in estimating K_1 (for one-tissue compartmental modeling) also followed similar results. In a study to estimate blood flow using a one-tissue compartmental modeling in that work, the SD relative reduction at the same bias was approximately 25% in the region with higher blood flow as compared to approximately 40% in the region with lower blood flow. These were also similar to what we found, i.e., SD relative reduction is more pronounced in the areas where there are less counts.

The possible future research may include applying our method to patient data. In this paper, the proposed method has been applied to myocardial blood flow estimation in a digitized phantom study. Applying the proposed algorithm in real data should also be investigated for further evaluation. Extending our PCG algorithm to two-tissue compartmental models can also be one of the future directions. In addition, motion correction is essential in *in vivo* dynamic PET imaging, especially in cardiac applications where the heart motion affects quantitation.[30] Including motion correction in our PCG-based

direct reconstruction would make it more practical for *in vivo* study.

5. CONCLUSION

We have proposed a novel preconditioner for direct PET parametric reconstruction based on the PCG approach. We applied our approach to a realistic cardiac simulation study to estimate the myocardial blood flow. The PCG with the proposed preconditioner increases significantly convergence rate of the reconstruction as compared to the CG. Our direct approach yields lower SD with the same bias as compared to the indirect approach. Such improvement is more pronounced for low-count studies and defect regions in the myocardium.

ACKNOWLEDGMENTS

The authors would like to thank the anonymous reviewers for their constructive comments, which greatly improved the paper. This work was supported in part by NIH (Grant No. NIH-HL110241).

[a]Present address: Martinos Center for Biomedical Imaging, Department of Radiology, Massachusetts General Hospital, Boston, Massachusetts 02114.
[b]Author to whom correspondence should be addressed. Electronic mail: elfakhri@pet.mgh.harvard.edu

[1]R. E. Carson, "Tracer kinetic modeling in PET," in *Positron Emission Tomography*, edited by D. L. Bailey, D. W. Townsend, P. E. Valk, and M. N. Maisey (Springer, London, 2005), pp. 127–159.
[2]A. Rahmim, J. Tang, and H. Zaidi, "Four-dimensional (4D) image reconstruction strategies in dynamic PET: Beyond conventional independent frame reconstruction," Med. Phys. **36**, 3654–3670 (2009).
[3]C. Tsoumpas, F. E. Turkheimer, and K. Thielemans, "A survey of approaches for direct parametric image reconstruction in emission tomography," Med. Phys. **35**, 3963–3971 (2008).
[4]D. L. Snyder, "Parameter estimation for dynamic studies in emission tomography systems having list-mode data," IEEE Trans. Nucl. Sci. **31**, 925–931 (1984).
[5]R. E. Carson and K. Lange, "The EM parametric image reconstruction algorithms," J. Am. Stat. Assoc. **80**, 20–22 (1985).
[6]H. H. Barrett, D. W. Wilson, and B. M. Tsui, "Noise properties of the EM algorithm: I. Theory," Phys. Med. Biol. **39**, 833–846 (1994).
[7]G. Wang and J. Qi, "Generalized algorithms for direct reconstruction of parametric images from dynamic PET data," IEEE Trans. Med. Imaging **28**, 1717–1726 (2009).
[8]J. Matthews, D. Bailey, P. Price, and V. Cunningham, "The direct calculation of parametric images from dynamic PET data using maximum-likelihood iterative reconstruction," Phys. Med. Biol. **42**, 1155–1173 (1997).
[9]S. R. Meikle, J. C. Matthews, V. J. Cunningham, D. L. Bailey, L. Livieratos, T. Jones, and P. Price, "Parametric image reconstruction using spectral analysis of PET projection data," Phys. Med. Biol. **43**, 651–666 (1998).
[10]A. J. Reader, F. C. Sureau, C. Comtat, R. Trebossen, and I. Buvat, "Joint estimation of dynamic PET images and temporal basis functions using fully 4D ML-EM," Phys. Med. Biol. **51**, 5455–5474 (2006).
[11]T. E. Nichols, J. Qi, E. Asma, and R. M. Leahy, "Spatiotemporal reconstruction of list-mode PET data," IEEE Trans. Med. Imaging **21**, 396–404 (2002).
[12]Q. Li, E. Asma, S. Ahn, and R. M. Leahy, "A fast fully 4D incremental gradient reconstruction algorithm for list mode PET data," IEEE Trans. Med. Imaging **26**, 58–67 (2007).
[13]G. Wang, L. Fu, and J. Qi, "Maximum a posteriori reconstruction of the Patlak parametric image from sinograms in dynamic PET," Phys. Med. Biol. **53**, 593–604 (2008).
[14]C. Tsoumpas, F. E. Turkheimer, and K. Thielemans, "Study of direct and indirect parametric estimation methods of linear models in dynamic positron emission tomography," Med. Phys. **35**, 1299–1309 (2008).
[15]Q. Li and R. M. Leahy, "Direct estimation of Patlak parameters from list mode PET data," *Proceedings of the Sixth IEEE International Symposium on Biomedical Imaging* (IEEE, 2009).
[16]G. Wang and J. Qi, "Acceleration of the direct reconstruction of linear parametric images using nested algorithms," Phys. Med. Biol. **55**, 1505–1517 (2010).
[17]A. Rahmim, Y. Zhou, J. Tang, L. Lu, V. Sossi, and D. F. Wong, "Direct 4D parametric imaging for linearized models of reversibly binding PET tracers using generalized AB-EM reconstruction," Phys. Med. Biol. **57**, 733–755 (2012).
[18]J. Yan, B. Planeta-Wilson, and R. E. Carson, "Direct 4D PET list mode parametric reconstruction with a novel EM algorithm," IEEE Trans. Med. Imaging **31**, 2213–2223 (2012).
[19]M. E. Kamasak, C. A. Bouman, E. D. Morris, and K. Sauer, "Direct reconstruction of kinetic parameter images from dynamic PET data," IEEE Trans. Med. Imaging **24**, 636–650 (2005).
[20]G. Wang and J. Qi, "An optimization transfer algorithm for nonlinear parametric image reconstruction from dynamic PET data," IEEE Trans. Med. Imaging **31**, 1977–1988 (2012).
[21]D. S. Lalush and B. M. W. Tsui, "The importance of preconditioners in fast Poisson based iterative reconstruction algorithms for SPECT," *IEEE Nuclear Science Symposium and Medical Imaging Conference* (IEEE, 1995).
[22]L. Kaufman, "Implementing and accelerating the EM algorithm for positron emission tomography," IEEE Trans. Med. Imaging **6**, 37–51 (1987).
[23]R. N. Gunn, A. A. Lammertsma, S. P. Hume, and V. J. Cunningham, "Parametric imaging of ligand-receptor binding in PET using a simplified reference region model," NeuroImage **6**, 279–287 (1997).
[24]E. U. Mumcuoglu, R. Leahy, S. R. Cherry, and Z. Zhou, "Fast gradient-based methods for Bayesian reconstruction of transmission and emission PET images," IEEE Trans. Med. Imaging **13**, 687–701 (1994).
[25]J. A. Fessler and S. D. Booth, "Conjugate-gradient preconditioning methods for shift-variant PET image reconstruction," IEEE Trans. Image Process **8**, 688–699 (1999).
[26]R. Clackdoyle and M. Defrise, "Tomographic reconstruction in the 21st century," IEEE Signal Process. Mag. **27**, 60–80 (2010).
[27]D. A. Bertsekas, *Nonlinear Programming* (Athena Scientific, 1999).
[28]W. P. Segars, "Development of a new dynamic NURBS-based cardiac torso (NCAT) phantom," Ph.D. thesis, University of North Carolina, 2000.
[29]M. D. Cerqueira, N. J. Weissman, V. Dilsizian, A. K. Jacobs, S. Kaul, W. K. Laskey, D. J. Pennell, J. A. Rumberger, T. Ryan, and M. S. Verani, "Standardized myocardial segmentation and nomenclature for tomographic imaging of the heart. A statement for healthcare professionals from the Cardiac Imaging Committee of the Council on Clinical Cardiology of the American Heart Association," Int. J. Cardiovasc. Imaging **18**, 539–542 (2002).
[30]M. Schwaiger, S. Ziegler, and S. G. Nekolla, "PET/CT: Challenge for nuclear cardiology," J. Nucl. Med. **46**, 1664–1678 (2005).